A Disposable and Self-Aligned 3-D Integrated Bio-Sensing Interface Module for CMOS Cell-Based Biosensor Applications

Joe L. Gonzalez, Paul K. Jo, Reza Abbaspour, and Muhannad S. Bakir

***Abstract*— This letter presents a disposable, self-aligned, and die-level socketed 3-D integrated biosensing-interface module (BIM) for biosensing applications. The enabling technologies of the BIM include: 1) mechanically flexible interconnects (MFIs) that provide temporary electrical interconnections to enable disposability; 2) sapphire precision balls and positive self-alignment structures, which in combination with KOH-etched pits provide the BIM self-alignment capabilities; and 3) a clamped socket that temporarily provides the necessary force for the MFIs to form and maintain electrical contact with the underlying test die during testing. Repeated alignment measurements show that the alignment of the BIM to the biosensor varies little between uses, hence demonstrating that the biosensor system can maintain accurate alignment. In addition, four-point resistance measurements were taken after assembly indicating that temporary electrical connections were formed and maintained.**

***Index Terms*— 3D IC, compliant interconnects, self-alignment, disposable biosensors, CMOS biosensors, cell-based bio-sensing.**

I. Introduction

CELL-BASED biosensing platforms, including CMOS biosensors, continue to impact pre-clinical pharmaceutical development, point-of-care testing, environmental monitoring, and pathogen detection [1]–[13]. CMOS cell-based biosensors in particular are attractive due to their high degree of integration, unparalleled signal processing, fast response, and low power, all at a potential low cost. Important for many CMOS cell-based biosensors in the aforementioned applications are the following: 1) high throughput, 2) minimal contamination (sterility assurance level (SAL) of 10^{-6}), 3) low cost, 4) large field-of-view, and 5) high resolution.

Currently, CMOS cell-based biosensors require post-fabrication processing typically due to the electrochemical instability of their surface electrodes (e.g., aluminum) in a saline-based medium and due to certain necessary surface treatments to improve cell adhesion and growth, all which serve to increase processing costs [3], [5], [14]–[16]. Throughput is also limited if the CMOS biosensor is reused as sterilization is necessary to minimize cross-contamination (and sterilization methods are limited as CMOS devices are present) [17], [18]. Disposing and replacing the biosensor is another (and more effective) option to circumvent cross contamination; however, this route is difficult/impractical as the biosensor is likely to be permanently attached and wire bonded to the package or board.

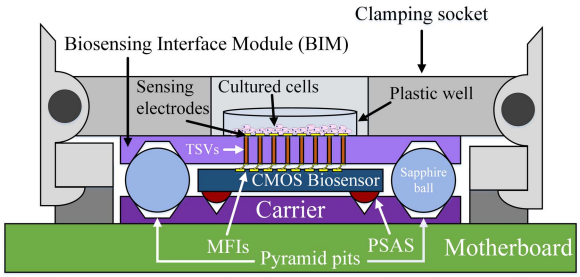

Fig. 1. Biosensing-interface module (BIM) in modular system.

In an attempt to address these challenges, this letter presents a disposable, self-aligned, and socketed biosensing-interface module (BIM), as seen in Figure 1, that serves to act as a 3D integrated interface between the underlying CMOS biosensor and the cells grown atop the surface. This electrical interface circumvents the need to post-process the CMOS biosensor while allowing for a quick and manual place-and-replace mechanism for high throughput testing. Additionally, as the BIM is scalable, high resolution and large field-of-view data is achievable. As few 3D packages for biosensing applications exist, such as the BIM presented here, the focus of this letter is on the die-level socketed module and hence, for demonstration purposes, the BIM is interfaced with a test die and not a CMOS biosensor.

The advantages associated with the presented BIM include the following: 1) self-alignment facilitates temporary interconnections, increases testing throughput as alignment placement tools are avoided, and enables field-deployable applications as a simple manual placement suffices for assembly, 2) temporary interconnections allow for the disposal of the BIM, which circumvents cross contamination, and hence leads to

Manuscript received May 15, 2018; revised June 19, 2018; accepted June 22, 2018. Date of publication July 2, 2018; date of current version July 24, 2018. This work was performed in part at the Georgia Tech Institute for Electronics and Nanotechnology, a member of the National Nanotechnology Coordinated Infrastructure, which is supported by the National Science Foundation under Grant ECCS-1542174. *(Corresponding author: Joe L. Gonzalez.)*

The authors are with the School of Electrical and Computer Engineering, Georgia Institute of Technology, Atlanta, GA 30318 USA (e-mail: joe.gonzalez@gatech.edu).

Color versions of one or more of the figures in this letter are available online at http://ieeexplore.ieee.org.

Digital Object Identifier 10.1109/LED.2018.2851969

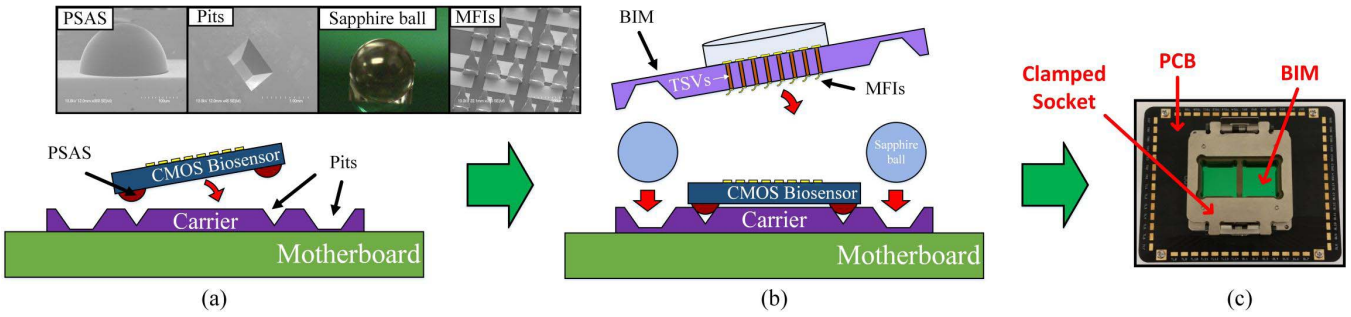

Fig. 2. Double self-alignment process flow demonstrating two levels of self-alignment: (a) CMOS biosensor to carrier self-alignment via a PSAS/pit mechanism, (b) BIM to carrier self-alignment via a sapphire ball/pit mechanism. Final clamped state (c) follows.

increased throughput as sterilization processes are avoided, and 3) since the BIM does not contain any CMOS devices, etc., it does not require a CMOS-only fabrication process, hence culture medium biocompatible materials and necessary surface treatments are easily incorporated into the overall fabrication process, which can potentially be performed at the wafer level, hence leading to decreased costs in accordance with economies of scale.

Our previous work introduced an "electronic-microplate" (e-microplate) that demonstrated preliminary data on the functionality of such an interface platform [19]. However, the e-microplate was not disposable/replaceable nor did it possess self-alignment capabilities. In contrast to the module introduced in this letter, permanent bonding using epoxy resin and flip-chip alignment/assembly were necessary to secure and position the e-microplate. Thus, we demonstrate: 1) self-alignment of the BIM to the underlying test die, which removes the need for an alignment/assembly placement tool, and corresponding alignment data, 2) an attachable/detachable clamp-socket based structure that compresses the BIM so that electrical connections are formed and maintained, and 3) temporary electrical connections between the BIM and the test die via mechanically flexible interconnects (MFIs) and corresponding four-point resistance data.

II. System Overview

As seen in Figure 1, the modular system is composed of: a carrier, a test die (or biosensor), the BIM, the clamped socket, and a PCB. The carrier contains self-alignment KOH-etched pits to self-align both the test die (via positive self-alignment structures or PSAS) and the BIM (via sapphire precision balls) [20], [21]. The BIM hence self-aligns to the test die via the carrier. The test die is also wire bonded to the carrier, which itself is wire bonded to the PCB for four-point resistance measurements (reported in Section III). After the BIM is self-aligned to the carrier and hence the test die, the clamp is inserted into its socket so that the BIM can electrically interconnect to the underlying test die electrodes via 58 μm pitch MFIs (a BIM contains two arrays of 1,024 MFIs) [22]–[24].

III. Setup, Results, and Discussion

A. Assembly and Alignment

To obtain self-alignment between the BIM and the test die, a double self-alignment mechanism was implemented:

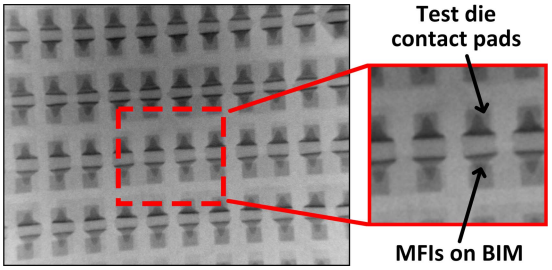

Fig. 3. X-ray image showing alignment between MFIs and corresponding electrodes on the test die.

1) self-alignment between the BIM and the carrier and 2) self-alignment between the test die and the carrier (both shown in Figure 1). The purpose of the carrier, as aforementioned, is to enable both levels of self-alignment and hence self-alignment between the BIM and the test die. To apply the necessary force onto the BIM so that the MFIs form an electrical connection, the clamp is inserted into the socket.

Different mechanisms enable each level of self-alignment as shown in Figure 2: 1) a PSAS-pit mechanism self-aligns the test die to the carrier and 2) a sapphire precision ball-pit mechanism self-aligns the BIM to the carrier. The pits are formed via KOH etching of ⟨100⟩ silicon (45% KOH at 90°C). The PSAS is fabricated via reflowing positive resist at a temperature above its glass transition temperature, T_g, as has been done in [20]. Due to the size of the pits, the misalignment tolerance during the initial assembly of the BIM is ±0.43 mm. The accuracy and repeatability of the self-alignment between BIM and test die is reported in Section III-B.

All assembly and alignment is performed via manual placement. Specifically, the carrier is manually picked up and placed into the socket, the test die is picked up and placed onto the carrier, the BIM is picked up and placed onto the carrier, and the clamp, as shown in Figure 2(c), is picked up and placed into the socket. Self-alignment occurs at every level with high accuracy as shown next in Section III-B.

B. Alignment Measurements and Alignment Repeatability

To measure the alignment accuracy between the BIM and the test die, X-ray images were first captured using a Dage X-Ray Inspection System (XD7600NT model), as shown in Figure 3. The Dage X-Ray built-in measurement tools are

TABLE I
SELF-ALIGNMENT REPEATABILITY MEASUREMENTS

Number of manually placed assemblies	Top Left (μm)		Top Right (μm)		Bottom Left (μm)		Bottom Right (μm)	
	x	*y*	*x*	*y*	*x*	*y*	*x*	*y*
1	-3-4	+3	-3-4	+3-4	-4	+3-4	-4	+3-4
10	-3-4	+3	-3-4	+3-4	-4	+3-4	-3-4	+3
20	-3-4	+3	-3	+3-4	-3-4	+3-4	-4	+3-4
50	-3-4	+3-4	-3-4	+3-4	-3-4	+3-4	-3-4	+3-4
100	-3-4	+3-4	-3-4	+3	-3-4	+3-4	-3	+3-4

then used to measure the misalignment from the X-ray images. To calibrate the X-ray tool, several features of known size were initially measured and all other measurements were scaled accordingly.

Alignment measurements are performed for each quarter of the MFI area array (top left, top right, bottom left, and bottom right). For each quarter, the x- and y- misalignment is recorded via measuring the distance (in the x- and y-directions) between the MFIs on the BIM and the electrodes on the test die. Several measurements were performed for each quarter (for both x- and y-) from which the average is computed and recorded, as shown in Table I. Initial alignment measurements demonstrate less than 5 μm of misalignment for every quarter (and each direction). Recall that the misalignment tolerance for manually placing the BIM onto the carrier is $\pm$0.43 mm ($\pm$430 μm).

Since the biosensor is intended for reuse, we performed multiple manually placed assemblies on the test die to test self-alignment repeatability. The results of these tests are also shown in Table I. As shown, 100 different manually placed assemblies are performed where the BIM is removed and then re-assembled onto the test die (and re-clamped). Little difference is observed between each self-alignment measurement, which demonstrates that self-alignment accuracy is consistent after repeated use. Self-alignment accuracy can be improved with better lithographic equipment and better lithographic alignment.

C. Electrical Data

To test the temporary electrical interconnections after the BIM is self-aligned, assembled, and clamped onto the test die, four-point resistance measurements of 2.1 μm thick MFIs were performed and recorded, as shown in Figure 4(a) and Figure 4(b). Figure 4(b) records several individual four-point IV curve measurements from one BIM sample; one is shown in Figure 4(a). As shown, an average of approximately 207.2 mΩ is recorded. Furthermore, the uniformity of this data (standard deviation of $\pm$10.1 mΩ) likely demonstrates that structural uniformity exists among the MFI structures and that a uniform assembly force is provided by the clamp. Modifying the gap between the BIM and test die (and the assembly force if necessary) will likely alter the contact resistance of the MFIs and hence their overall resistance.

These resistance measurements demonstrate that self-alignment is successfully achieved (as also seen previously via the alignment data) and that a sufficient assembly force is applied, hence an electrical connection can be formed and maintained (and removed at any time). The implications of these results convey that the potential exists for the development of a high-resolution, large field-of-view CMOS cell-based biosensor system that is field-deployable and that has the ability to deliver high-throughput testing.

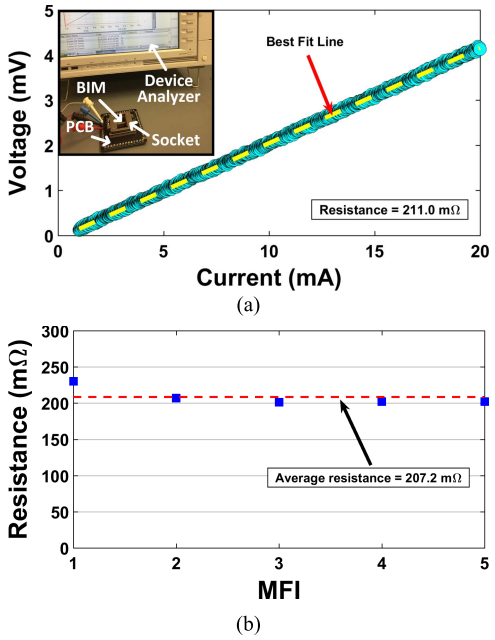

Fig. 4. (a) Four-point resistance setup and extracted resistance from an IV curve of one of the MFIs on the BIM and (b) four-point resistance measurements (including contact resistance) for five different MFIs (2.1 μm thick) on the same BIM sample.

IV. CONCLUSION

A 3D integrated, self-aligned, and die-level socketed biosensing-interface module (BIM) was microfabricated for CMOS cell-based biosensor applications. The enabling technologies of the BIM allowed for 1) the self-alignment of the BIM upon manual placement, achieving an alignment accuracy of better than 5 μm, and 2) the ability to form and maintain temporary electrical interconnections. An average of 207.2 mΩ four-point resistance for 2.1 μm thick MFIs was recorded. Given these capabilities, the BIM has potential to assist in a wide variety of biosensing applications.

REFERENCES

[1] R. Zang, D. Li, I.-C. Tang, J. Wang, and S.-T. Yang, "Cell-based assays in high-throughput screening for drug discovery," *Int. J. Biotechnol. Wellness Industries*, vol. 1, no. 1, pp. 31–51, Apr. 2012, doi: 10.6000/1927-3037.2012.01.01.02.

[2] Q. Gui, T. Lawson, S. Shan, L. Yan, and Y. Liu, "The application of whole cell-based biosensors for use in environmental analysis and in medical diagnostics," *Sensors*, vol. 17, no. 7, p. 1623, Jul. 2017, doi: 10.3390/s17071623.

[3] T. Chi, J. S. Park, J. C. Butts, T. A. Hookway, A. Su, C. Zhu, M. P. Styczynski, T. C. McDevitt, and H. Wang, "A multi-modality CMOS sensor array for cell-based assay and drug screening," *IEEE Trans. Biomed. Circuits Syst.*, vol. 9, no. 6, pp. 801–814, Dec. 2015, doi: 10.1109/TBCAS.2015.2504984.

[4] H. Wang, A. Mahdavi, D. A. Tirrell, and A. Hajimiri, "A magnetic cell-based sensor," *Lab Chip*, vol. 12, no. 21, pp. 4465–4471, Oct. 2012, doi: 10.1039/C2LC40392G.

[5] Q. Liu and P. Wang, *Cell-Based Biosensors: Principles and Applications*. Norwood, MA, USA: Artech House, 2009.

[6] Q. Liu, C. Wu, H. Cai, N. Hu, J. Zhou, and P. Wang, "Cell-based biosensors and their application in biomedicine," *Chem. Rev.*, vol. 114, no. 12, pp. 6423–6461, Jun. 2014, doi: 10.1021/cr2003129.

[7] N. Raut, G. O'Connor, P. Pasini, and S. Daunert, "Engineered cells as biosensing systems in biomedical analysis," *Anal. Bioanal. Chem.*, vol. 402, no. 10, pp. 3147–3159, Apr. 2012, doi: 10.1007/s00216-012-5756-6.

[8] Y. Adiguzel and H. Kulah, "CMOS cell sensors for point-of-care diagnostics," *Sensors*, vol. 12, no. 8, pp. 10042–10066, Jul. 2012, doi: 10.3390/s120810042.

[9] Y. Lu, D. Macias, Z. S. Dean, N. R. Kreger, and P. K. Wong, "A UAV-mounted whole cell biosensor system for environmental monitoring applications," *IEEE Trans. Nanobiosci.*, vol. 14, no. 8, pp. 811–817, Dec. 2015, doi: 10.1109/TNB.2015.2478481.

[10] L. Tan and K. Schirmer, "Cell culture-based biosensing techniques for detecting toxicity in water," *Current Opinion Biotechnol.*, vol. 45, pp. 59–68, Jun. 2017, doi: 10.1016/j.copbio.2016.11.026.

[11] P. Banerjee and A. K. Bhunia, "Cell-based biosensor for rapid screening of pathogens and toxins," *Biosensor Bioelectron.*, vol. 26, no. 1, pp. 99–106, Sep. 2010, doi: 10.1016/j.bios.2010.05.020.

[12] P. Banerjee and A. K. Bhunia, "Mammalian cell-based biosensors for pathogens and toxins," *Trends Biotechnol.*, vol. 27, no. 3, pp. 179–188, Mar. 2009, doi: 10.1016/j.tibtech.2008.11.006.

[13] C. M. Lopez, H. S. Chun, L. Berti, S. Wang, J. Putzeys, C. Van Den Bulcke, J. W. Weijers, A. Firrincieli, V. Reumers, D. Braeken, and N. Van Helleputte, "A 16384-electrode 1024-channel multimodal CMOS MEA for high-throughput intracellular action potential measurements and impedance spectroscopy in drug-screening applications," in *IEEE Int. Solid-State Circuits Conf. (ISSCC) Dig. Tech. Papers*, Feb. 2018, pp. 464–466, doi: 10.1109/ISSCC.2018.8310385.

[14] A. H. Graham, J. Robbins, C. R. Bowen, and J. Taylor, "Commercialisation of CMOS integrated circuit technology in multi-electrode arrays for neuroscience and cell-based biosensors," *Sensors*, vol. 11, no. 5, pp. 4943–4971, May 2011, doi: 10.3390/s110504943.

[15] J. S. Park, M. K. Aziz, S. Li, T. Chi, S. I. Grijalva, J. H. Sung, H. C. Cho, and H. Wang, "1024-pixel CMOS multimodality joint cellular sensor/stimulator array for real-time holistic cellular characterization and cell-based drug screening," *IEEE Trans. Biomed. Circuits Syst.*, vol. 12, no. 1, pp. 80–94, Feb. 2018, doi: 10.1109/TBCAS.2017.2759220.

[16] J. Park, M. K. Aziz, S. Gonzalez, D. Jung, T. Chi, S. Li, H. C. Cho, and H. Wang, "A CMOS 22k-pixel single-cell resolution multi-modality real-time cellular sensing array," in *Proc. IEEE Custom Integr. Circuits Conf. (CICC)*, Apr. 2017, pp. 1–4, doi: 10.1109/CICC.2017.7993710.

[17] J. Irudayaraj, Ed., *Biomedical Nanosensors*. New York, NY, USA: Pan Stanford, 2012.

[18] B. J. Lambert, T. A. Mendelson, and M. D. Craven, "Radiation and ethylene oxide terminal sterilization experiences with drug eluting stent products," *AAPS PharmSciTech*, vol. 12, no. 4, pp. 1116–1126, Dec. 2011, doi: 10.1208/s12249-011-9644-8.

[19] M. Zia, T. Chi, C. Zhang, P. Thadesar, T. Hookway, J. Gonzalez, T. McDevitt, H. Wang, and M. S. Bakir, "A microfabricated electronic microplate platform for low-cost repeatable biosensing applications," in *IEDM Tech. Dig.*, Dec. 2015, pp. 29.4.1–29.4.4, doi: 10.1109/IEDM.2015.7409794.

[20] H. S. Yang, C. Zhang, and M. S. Bakir, "Self-alignment structures for heterogeneous 3D integration," in *Proc. IEEE 63rd Electron. Compon. Technol. Conf.*, May 2013, pp. 232–239, doi: 10.1109/ECTC.2013.6575577.

[21] J. E. Cunningham, A. V. Krishnamoorthy, I. Shubin, X. Zheng, M. Asghari, D. Feng, and J. G. Mitchell, "Aligning chips face-to-face for dense capacitive and optical communication," *IEEE Trans. Adv. Packag.*, vol. 33, no. 2, pp. 389–397, May 2010, doi: 10.1109/TADVP.2009.2037437.

[22] C. Zhang, H. S. Yang, and M. S. Bakir, "Highly elastic gold passivated mechanically flexible interconnects," *IEEE Trans. Compon., Packag., Manuf. Technol.*, vol. 3, no. 10, pp. 1632–1639, Oct. 2013, doi: 10.1109/TCPMT.2013.2276436.

[23] C. Zhang, H. S. Yang, and M. S. Bakir, "Mechanically flexible interconnects (MFIs) with highly scalable pitch," *J. Micromech. Microeng.*, vol. 24, no. 5, p. 055024, May 2014, doi: 10.1088/0960-1317/24/5/055024.

[24] C. Zhang, H. S. Yang, H. D. Thacker, I. Shubin, J. E. Cunningham, and M. S. Bakir, "Mechanically flexible interconnects with contact tip for rematable heterogeneous system integration," *IEEE Trans. Compon., Packag., Manuf. Technol.*, vol. 6, no. 11, pp. 1587–1594, Oct. 2016, doi: 10.1109/TCPMT.2016.2614997.